A new method for mapping spatial resolution in compound eyes suggests two visual streaks in fiddler crabs

Zahra M. Bagheri [1, *], Anna-Lee Jessop [1], Susumu Kato[1], Julian C. Partridge[3,] Jeremy Shaw[2], Yuri Ogawa[1] and Jan M. Hemmi [1, 3, *]

[1] School of Biological Sciences, the University of Western Australia, Perth, Australia

[2] Centre for Microscopy, Characterisation and Analysis, the University of Western Australia, Perth, Australia

[3] The UWA Oceans Institute, the University of Western Australia, Perth, Australia

Correspondence: Zahra.bagheri@uwa.edu.au, jan.hemmi@uwa.edu.au

Abstract

Visual systems play a vital role in guiding the behaviour of animals. Understanding the visual information animals are able to acquire is therefore key to understanding their visually-mediated decision making. Compound eyes, the dominant eye type in arthropods, are inherently low-resolution structures. Their ability to resolve spatial detail depends on sampling resolution (interommatidial angle) and the quality of ommatidial optics. Current techniques for estimating interommatidial angles are difficult, and generally require *in vivo* measurements. Here, we present a new method for estimating interommatidial angles based on the detailed analysis of 3D Micro-CT images of fixed samples. Using custom-made MATLAB software we determine the optical axes of individual ommatidia and project these axes into the three-dimensional space around the animal. The combined viewing directions of all ommatidia, estimated from geometrical optics, allow us to estimate interommatidial angles and map the animal's sampling resolution across its entire visual field. The resulting topographic representations of visual acuity match very closely the previously published data obtained from both fiddler and grapsid crabs. However, the new method provides additional detail that was not previously detectable and reveals that fiddler crabs, rather than having a single horizontal visual streak as is common in flat world inhabitants, likely have two parallel streaks located just above and below the visual horizon. A key advantage of our approach is that it can be used on appropriately preserved specimens allowing the technique to be applied to animals such as deep-sea crustaceans that are inaccessible or unsuitable for *in vivo* approaches.

Keywords: Fiddler crab, compound eye, eye map, visual resolution, visual ecology

1. Introduction

Vision is the primary sense used by many animals for a wide range of behaviours including mating, navigating, feeding, avoiding predators, and many other functions (Land and Nilsson, 2012). Nevertheless, across the animal kingdom, there is a marked diversity in the structure and 'design' of visual systems, reflecting both the constraints of animals' phylogenetic histories as well as those imposed by their visual environments.

Among arthropods, compound eyes are the dominant eye type. Compound eyes are composed of many hundreds, or thousands, of tiny independent photosensitive units (ommatidia) each with its own corneal facet, crystaline cone lens, and light detecting cells. The structure of these types of eyes inevitably confer low-resolution but have the advantage that they allow flexible control over the shape and extent of the visual field. As a result, the spatial detail that can be resolved often varies across the visual field, allowing information capture to be optimised for key visual tasks that species need to perform.

The ability of compound eyes to resolve spatial detail depends essentially on two factors: the fineness of the mosaic of receptive elements that sample the image (measured as the interommatidial angle), and the spatial cut-off frequency of the optics (Land, 1989). Smaller interommatidial angles allow the retina to detect smaller features in the imaged scene (Kirschfeld, 1976; Land, 1981; Warrant and McIntyre, 1993). Larger facet diameters (D) lead to an increase in the optical cut-off frequency as well as an increased sensitivity to light (Kirschfeld, 1976; Land, 1981). An eye of a given size cannot simultaneously maximise both its resolution and sensitivity while maintaining the extent of its visual field (Land 1997). As a consequence, many compound eyes have modest overall resolution but are equipped with distinct regional specialisations, including parts with higher than average resolution. In many arthropods, for example crabs (Zeil and Al-Mutairi 1996), back swimmers (Schwind 1980), and water striders (Dahmen 1991), which spend important stages of their lives in habitats that are mostly confined to a flat horizontal plane, a 'visual streak' of high resolution is found along the visual horizon. Such a visual streak is thought to help these animals detect conspecifics, predators, or prey within the part of the visual field where they are most likely to occur (Zeil and Al-Mutairi 1996; Zeil and Hemmi, 2006). In other invertebrates, such as predatory and mate-chasing insects, a more or less upward looking 'acute zone' has been shown to be an adaptive specialisation for this form of target tracking (Land, 1989). In contrast to acute zones, 'bright zones', such as are found in the eyes of blowfly (van Hateren et al., 1989) and hoverfly

(Straw et al., 2006), improve contrast sensitivity by increasing facet size and therefore light capture. However, spatial resolution is not increased as the ommatidia of bright zones do not also have smaller interommatidial angles (van Hateren et al., 1989; Straw et al., 2006). Identifying the distribution of such different regional specialisations and the global 'design' of animal eyes is key to understanding the ecology of vision of animals and the evolutionary drivers underpinning both sensory processing and visually-mediated behavioural strategies.

To date, two key methods have been developed to measure interommatidial angles in compound eyes: pseudopupil analysis (Horridge, 1978), and the radius of curvature method (Bergman and Rutowski, 2016).

The pseudopupil analytical approach takes advantage of the fact that in (many) compound eyes a black spot can be seen on the eye's surface, where the optical axes of ommatidia are directed towards the observer. By moving the observer's position relative to the animal's eye, the pseudopupil can be tracked and its position with respect to the ommatidial facets can be used to measure interommatidial angles and ommatidial viewing directions. The advantage of this method is that it directly measures the direction of the optical axis of the ommatidia. However, the analysis requires a live animal in which the pseudopupil is clearly visible. Moreover, the precision of the method is limited by the observing optical equipment which determines the size of the pseudopupil and therefore the resolution at which changes in interommatidial angles can be measured (Land,1997).

The radius of curvature method uses the local eye radius and the diameter of individual facets to estimate interommatidial angles. This method has proven to be reasonably accurate when used to measure interommatidial angles in two species of butterflies (Bergman and Rutowski, 2016). More recently, Taylor et al. (2019) applied the radius of curvature method to microCT images to analyse the visual resolution in the compound eyes of bumblebees and honeybees, and generally found good agreement with previously published data. However, this method does not utilise the full power of 3D imaging as the radius of curvature only considers the external shape of the eye and does not take to account the arrangement of the crystalline cones. More generally, in compound eyes that deviate from a spherical shape, as many compound eyes do, this method will lead to poor estimates of spatial resolution as the ommatidia are often not aligned perpendicularly to the local external curvature of the eye. Therefore, the radius of curvature method is limited to more or less spherical compound eyes.

Here, we present a new method for estimating interommatidial angles based on 3D microCT image stacks. This method allows the viewing direction of each individual ommatidium to be estimated. It does not depend on access to live animals, nor the presence of a clear pseudopupil, and is not limited to spherically-symmetrical compound eyes. We use fiddler crabs and grapsid crabs as well-studied animal models to explain the method and highlight details in the spatial distribution of the crab's ommatidia that were not previously detected due to the spatial smoothing inherent in the pseudopupil method (Smolka and Hemmi, 2009; Zeil, 1996; Land and Layne, 1995; Zeil et al, 1986).

Previous studies on fiddler crabs (Smolka and Hemmi, 2009; Land & Layne, 1995; Zeil, 1996; Zeil et al, 1986) and grapsid crabs (De Astrada et al., 2012, Zeil et al, 1986) have shown the presence of a strong horizontal streak of high resolution which is approximately aligned with the visual horizon. In addition, there are clear regional differences in resolving power between the dorsal, ventral and central visual fields. The result of applying our new method in two fiddler crab species and one species of grapsid crabs shows good agreement with previously published data in terms of field of view and regional specialisations. However, the results suggest that the visual streak in fiddler crabs is, instead, composed of two close by streaks located just above and below the visual horizon.

2. Materials and Methods

2.1. Animals

Two fiddler crabs, a male *Gelasimus dampieri* (formerly *Uca dampieri*), and a female *Tubuca flammula* (formerly *Uca flammula*), as well as one grapsid crab, a male *Neohelice granulata* (formerly *Chasmagnathus granulatus*) were used in this study (the sizes of the specimens were 19.52mm, 31.3mm, and approximately 28mm carapace width, respectively, measured between lateral carapace spines). Both fiddler crabs were collected from intertidal mudflats near Learmonth (22°18S, 114°9E), south of Exmouth, Western Australia, and the *N. granulata* was collected from narrow coastal inlets of San Clemente del Tuyú, Argentina. The fiddler crabs were housed in an artificial mudflat in the laboratory at the University of Western Australia before preparation. In the artificial mudflat the crabs were exposed to a tidal cycle of seawater inundation, were maintained under a daily light 12L:12D light regime that includes UV and their diet was supplemented with fish food. Freshly caught *N. granulata* were transported to the laboratory at the university of Buenos Aires where they were lodged in plastic tanks filled

with seawater under a daily light 12L:12D light regime. A fixed eye of *N. granulata* was supplied by Martín Berón de Astrada for microCT scanning.

2.2. Sample preparation and scanning

Fiddler crabs were euthanised by UWA AEC approved methods (UWA AEC project number RA/3/100/1515) by being immersed in iced seawater for 5 min. Dissections, carried out immediately after euthanasia, were performed by removing the eyestalk at the base and immediately fixing it in 4% paraformaldehyde in 0.1 M phosphate buffer (pH 7.2) at room temperature for 2 min. The compound eye was then separated from the eyestalk, leaving a 3 mm stub and processed by fixation at 4°C for at least 12 hours. As contrast in X-ray imaging is dependent on the differential absorption of X-rays by features within the sample, the contrast of tissues within the eye stalk was enhanced by staining with an aqueous iodine/potassium iodide solution (I2K) for 12 hours. The stain was used at a concentration of 1% w/v iodine and 2% w/v potassium iodide, prepared by diluting a stock solution of 5% and 10% I2K, respectively using deionised (DI) water. The eyestalk was then rinsed in DI water (3x 10 min). The *G. dampieri* sample was placed into a tip-sealed 200 µL pipette tip loaded with DI water. The pipette tip was centrifuged at 664 g for 20s to ensure the sample was seated securely within the tube. For the *T. flammula* and *N. granulata* samples, agarose, rather than DI water, was placed into the pipette tip and left at 25°C to cool and form a gel for 30 minutes before scanning. The other end of the pipette tip was sealed with putty (Blu-Tack, Bostik) to prevent sample dehydration and the pipette tip was mounted on a holder for X-ray micro-Computed Tomography (microCT).

The specimens were scanned with a microCT system (Versa 520 XRM, Zeiss, Pleasanton, CA) running Scout and Scan software (v11.1.5707.17179). Scans were conducted at a voltage of 40kV and 3W (70 kV and 6W for *N. granulata* sample), using the LE1 beam filter. 4x optical magnification and 2x camera binning were used with source and detector positions set to deliver an isotropic voxel size of 2.9 µm. A total of 3201 projections were collected over 360°, each with an exposure time of 5s.

Raw projection data were reconstructed using XMReconstructor software (v10.7.3679.13921, Zeiss) following a standard centre shift and beam hardening (0.1) correction. The standard 0.7 kernel size reconstruction filter setting was also used.

2.3. Analysis

Optical axes: Using custom-made software written in MATLAB 2015b (The MathWorks, Inc.) we manually marked the centre of the corneal facet and the centre of the distal tip of the rhabdom (located at the base of the crystalline cone in fiddler crabs) of each individual ommatidium in microCT reconstructed images (Figure 1). Select corneal points were matched with their corresponding rhabdom points by carefully aligning the selected ommatidia within three perpendicular planes (Figure 1A-C) and adjusting the contrast to visualise the crystalline cones. The remainder of the rhabdomal points were then matched with corneal points according to their spatial relationships. The custom-made software allows extraction of the position of these centres in 3-dimensional space. Using the marked points, we reconstructed the eye structure and calculated the 3D optical axes (strictly speaking, the optical axes of the crystalline cones) of individual ommatidia (Figure 1D). Each individual ommatidium was labelled with horizontal row and vertical column numbers (Figure 2A) which were used to identify the neighbouring ommatidia in subsequent processing.

Sampling resolution: The fineness of the mosaic of retinal receptive elements that sample an image is mostly described in terms of the spatial sampling frequency of the mosaic, which largely determines its spatial resolution. A commonly used measure to quantify spatial resolution of compound eyes is the interommatidial angle. This angle, measured between adjacent ommatidia, often varies across the eye and, due to the packing of ommatidia, typically shows difference when measured in different directions (e.g. horizontal or vertical). We determined the vertical interommatidial angle ($\Delta\varphi_v$) by calculating the vertical angle between the optical axes of horizontal rows of ommatidia (Figure 2A, B). In the horizontal direction we calculated interommatidial angle ($\Delta\varphi_h$) as half the angle between the optical axes of neighbouring ommatidia along each row (Figure 2A, B; also see Stavenga, 1979). The sampling resolution (cycles/°; c/°) in each direction (vertical or horizontal) is then calculated as the reciprocal of twice the interommatidial angle $v_s=1/(2\Delta\varphi)$ (Land, 1997).

Optical resolution: The highest spatial frequencies, representing the finest details in a visual scene, are usually lost when a scene is imaged onto the retina of an eye. The receptive field of individual photoreceptors (usually described by the half width, $\Delta\rho$, of their acceptance angle) is a determining factor in angular sensitivity and therefore resolving power of an eye. For instance, when viewing a black and white grating, if the receptive field of a receptor is wider than a single stripe, any stripes that can fit into the receptor's diameter will not be resolved

separately, and there is, therefore, a loss of spatial information. In consequence, contrast reduces as spatial frequencies increase until it reaches zero at the spatial cut-off frequency (Snyder, 1979; Warrant and McIntyre, 1993).

Diffraction which arises from the wave nature of light sets the cut-off frequency. When light from a point source reaches a lens as a wavefront, the central region of the wavefront is delayed more than the edge region. This phenomenon leads to the formation of a blurred area in the image, known as the Airy disc or diffraction pattern. In wave optics the limit to image quality is set by diffraction, specifically by the angle subtended by the Airy disc. Under a point source of monochromatic light (wavelength λ), the cut-off frequency (v_{co}), which is a measure of the finest resolvable spatial frequency, is directly related to the lens diameter, *D*, and inversely to wavelength, thus: $v_{co} = D/1.02\lambda$.

The acceptance angle of an ommatidium in a compound eye can be approximated by the half width of the Airy disc if: (1) the eye is strongly light adapted; (2) the rhabdom is very thin and propagates mostly the fundamental waveguide mode (3) the lens has a relatively large focal length to diameter ratio (*f/D*>2) (Stavenga, 2003a; Stavenga, 2003b; Stavenga, 2004). In both *G. dampieri* (*f/D*= 5.00± 0.80) and *T. flammula* (*f/D*= 6.24± 0.76) these conditions are satisfied. Therefore, we have used Airy disc half-widths to estimate acceptance angles. The facet diameter (*D*, in µm) was estimated as the diameter of the incircle of hexagonal facet which was calculated as the average distance of the centre of facet from the centres of six neighbouring ommatidia (Figure 2C).

3. Results

3.1. Field of view and distribution of ommatidia

In total, 9715 ommatidia were identified and labelled in the microCT images of *G. dampieri*. In most cases, the positions of the centre of the corneal facet and the centre of the distal tip of the rhabdom were easily visible, especially near the eye equator where the facets and ommatidia are generally large. Although the ommatidia are clearly visible in the microCT images right to the edge of the eye border, the ommatidia become smaller and less regularly arranged closer to the edge. This make it more difficult to accurately determine the 3D positions of the distal tip of the rhabdoms, the locations of which are required to reconstruct the optical axes of the crystalline cones. However, we are confident that we were able to identify and measure all ommatidia, with the exception of a few ommatidia at the very edge of the array

that could not be adequately interpreted, possibly representing ommatidia in an early phase of development.

Figure 3 shows the visual field for the right eye of *G. dampieri* estimated by mapping the optical axes of individual ommatidia into a sphere. The raw data (Supplementary Figure S1) were smoothed using a smoothing spline based on the discrete cosine transform (see Garcia, 2010 for details of the smoothing method). The visual horizon was determined by rotating the eye (no translation is involved) so the streak's plane becomes horizontal. This also results in the ommatidial rows becoming almost horizontal across the centre of the eye. The frontal, lateral and medial directions were determined by using the landmarks on the eye outline. Horizontally, the visual field covers a full 360º field of view between -10º to 50º of elevation. However, the extent of the field of view varies considerably in the dorso-ventral direction, covering a range of elevations from -50º to 80º in the frontal and lateral directions, and reducing to -40º to 70º in the caudal, and -10º to 70º in the medial, directions. Moreover, there is approximately a 30º overlap of the visual field in the medial direction, meaning that ommatidia from two medial borders of the eye project into the same part of the visual field.

Although the visual field covers almost 72% of the dorso-ventral axis, the ommatidia are not evenly distributed along this axis. Indeed, most facets look into a very narrow band around the visual horizon. 30% of ommatidia are looking at ±9º of elevation and 50% are devoted to ±18º of elevation (Figure S2).

3.2. Sampling Resolution

There is a clear 'streak' of high vertical sampling resolution along the visual horizon at approximately 5º above the horizon (Figure 4 A, B). Within the horizontal acute zone, the area with maximum resolving power of 1.92 c/° is located in the azimuth range 30º- 60º. The vertical sampling resolution reduces to 1.42 c/°, 1.25 c/°, 0.92 c/° and 0.22 c/° in the frontal, lateral, caudal and the posterior–medial areas respectively.

Away from the primary horizontal streak, vertical resolution decreases sharply towards more dorsal directions of view. However, in the ventral direction another horizontally orientated streak of high resolution (the secondary streak), albeit less pronounced than the first streak, is found in the frontal-lateral rim between -5º to -10º of elevation. The maximum resolution of the eye in this streak is 0.74 c/° (Figure 4A, B) and is separated from the primary visual streak by 10-15 degrees and a region of the eye with a resolution of ca. 0.45 c/°. Below the secondary streak resolution falls to around 0.2 c/° in the ventral field of view.

The vertical elongation of the eye of the crab leads to smaller vertical interommatidial angles, and thus to increased vertical sampling resolution throughout this visual streak. In contrast, horizontal resolution (Figure 4C, D) is not markedly elevated; indeed, the horizontal resolution is almost uniform across the eye with only a slight increase in the lateral field of view, and/or lateral ommatidia.

Since this 'secondary streak' has not been reported previously in any species of fiddler crab, we extended the observations made in *G. dampieri* to a female *T. flammula*, to investigate the potential existence of this 'secondary streak' in another species of fiddler crab. We labelled 13800 ommatidia covering most of the eye except a small region in the medial area. The secondary visual streak is also obvious in *T. flammula* (Figure 5A, B). The secondary streak is at ~10° above the horizon, while the primary streak (the visual streak with higher vertical resolution) sits on the horizon in the frontal-lateral-caudal (0° to 150°) areas. However, the primary streak merges with the secondary one in both the fronto-medial (-30° to -60°) and caudal areas (150° to 180°). The vertical resolution of the secondary streak varies between 0.9-1.3 c/°in frontal-caudal areas with the peaks at 20° and 140°. In contrast to *G. dampieri*, the vertical sampling resolution of the more ventral streak is higher than that of the more dorsal streak. Moreover, the primary (more ventral) visual streak shows two peaks in vertical resolution: one frontally (0°) and one laterally (30°-90°) located with sampling resolution maxima of 1.6 c/° and 1.5 c/°, respectively. However, the 'hot spot' of vertical resolution appears to be where the two streaks merge (between 0° and -30° in azimuth) with a maximum of 1.99 c/°. Further figures for *T. flammula*, including those showing horizontal resolution, are provided in the Supplementary data (Figures S3).

Given the surprising observation of a secondary streak in both species of fiddler crabs, we also labelled 5000 ommatidia in the fronto-lateral part of the eye of a male *N. granulata* which has a slightly different eye shape compared to fiddler crabs (more spherical and less elongated). The spatial resolution of *N. granulta* has been the subject of a careful optical reconstruction based on the pseudo-pupil method (De Astrada et al., 2012). Unlike the two fiddler crab species that we tested here, we found only one visual 'streak' of high vertical sampling resolution. The streak is positioned at approximately 10º above the horizon (Figure 5C, D). The vertical resolution of this streak varies between 1.3-1.93 c/° in the fronto-lateral area of the eye and peaks at an azimuth of approximately 30°. Similar to previous measurements in *N. granulata* (De Astrada et al., 2012) the vertical sampling resolution decreases more sharply towards dorsal compared to ventral directions of view. The horizontal resolution (Figure 5E, F) is not

uniform across the eye and increases towards the lateral side of the eye with a maximum of 0.63 c/° at an azimuth of approximately 90° (refer to Supplementary data, Figures S4 for map of optical axes and facet diameter of *N. granulata*).

3.3. The location of visual streak and the surface normal of the eye

The method employed in this reconstruction of visual fields is potentially sensitive to fixation artefacts. One way to check whether the double visual streak of the fiddler crabs or the unusually high (10°) elevation of the visual streak of *N. granulata* is a result of eye distortions is to project the sampling resolution back onto the eye and identify the ommatidia that form the visual streak. If the high visual streak of *N. granulata* were caused by an internal tissue shrinkage of the eye, for instance, then the ommatidia that form the visual steak should sit low on the eye. Figures 6A, B, C show a clear correlation between the elevations of the streaks in the world coordinates with their vertical position on the eyes. In all cases, the streaks that are high in elevation are also very high on the eye and parts of the eye that project to the horizon are relatively central on the eye. In addition, we calculated the angle between the local surface normal of the eye and the optical axes of the ommatidia (Figure 6D, E, F). We would expect that in this high-resolution zone of the eye, the optical axes of ommatidia should be arranged approximately perpendicular to the surface of the eye in order to limit reflections and improve optical performance. In all three animals all visual streaks reside almost completely inside the flat part of the eye where angular differences between ommatidial axes and the local surface normal of the eye are less than 3°, clearly arguing against major eye distortions. As expected, in all animals, deviation from surface normal increases sharply where the eye curvature increases. However, in the ventral area, below the visual streak deviations from surface normal develop more gradually than dorsally. This asymmetry correlates with the sharper decrease of sampling resolution in the dorsal compared to the ventral visual field (Figure 4, 5 and De Astrada et al., 2012). The deviation from surface normal in the ventral part of the eye can go as high as 16°. Irrespective of the vertical position of the visual streak(s), all animals have their biggest facets at approximately 5° above the horizon in the lateral direction (Figure 6 G, H, I, see also Section 3.4 and Supplementary Figures S3, S4), located approximately in the middle of the elongated eye space.

3.4. Facet Diameter and Optical Resolution

In addition to sampling resolution (determined by receptor spacing), the resolving power of compound eyes is also limited by diffraction at the facet lenses (Land, 1989). Larger facet diameters reduce diffraction, which leads to improved optical quality (Land, 1989), resulting in images with higher contrasts at high spatial frequencies. The effect of lens diameter on resolution can be expressed as the cut-off frequency v_{co} (measured in c/°), the spatial frequency at which image contrast reaches zero. The cut-off frequency has an inverse relationship with the receptive field of photoreceptors ($v_{co}=1/\Delta\rho$, Snyder, 1979; Warrant and McIntyre, 1993). As is described in the Methods (Section 2.3), the acceptance angle in compound eyes with facet geometry such as is found in fiddler crabs can be approximated by the half width of the Airy disc of each ommatidium, which depends only on the diameter of the facet lenses and the wavelength of sampled light.

Facet diameters (Figure 6G, 7A), and therefore optical resolution across the eye, have a more uniform distribution compared to sampling resolution (Figure 7B,C). Facets are largest in ommatidia having fields of view at -5° to 20° of elevation, which coincides with the primary streak. The facets with greatest diameters (D=32.3±0.32 µm, ±s.d.) are located in a narrow strip in the lateral part of the eye at angles of 60°-150° in azimuth. The facet diameters reduce to 30.4±0.68 µm in the frontal area. The smallest measured facets (16±1.52 µm) are in the dorsal and ventral areas of the eye between the frontal (0°) and the medial (-90°) part of visual field. Direct comparison of sampling resolution versus optical resolution for different wavelengths (Figure 7B, C) suggests that the lateral region of the eye is able to resolve spatial patterns at longer wavelengths than the frontal visual field.

4. Discussion

Here, we present a new method, based on 3D microCT image stacks of compound eyes, which can be used to reconstruct the viewing directions of individual ommatidia and create maps of sampling and optical resolution across the eye's entire visual field.

4.1. Comparison to other studies

Overall, the magnitude and spatial distribution of the calculated sampling resolution in *G. dampieri* closely resembles that of its sister species *G. vomeris*, for which independent

measurements based on the pseudopupil method have been obtained, (Smolka and Hemmi, 2009), with a slightly higher vertical sampling resolution in *G. dampieri* (1.92 c/° vs 1.54 c/°). Smolka and Hemmi (2009) reported two distinct areas of high resolving power within the visual streak of *G. vomeris*; one in the frontal zone (0° in azimuth) and the second one in the lateral visual field (60°-90° in azimuth). Although we observe the same pattern in *T. flammula*, the visual field of *G. dampieri* shows only one distinct area of high acuity (between 30°-60° azimuth) along the horizontal extent of the primary visual streak. However, the relative changes between optical and sampling resolution in the frontal and lateral visual field in *G. dampieri* (Figure 7B, C) very closely match those that were reported by Smolka and Hemmi (2009) for *G. vomeris*.

The relatively uniform horizontal sampling resolution found in both *G. dampieri* and *T. flammula* (Figure 4 and Figure S3, Supplementary Material) also agrees well with previous studies on fiddler crabs (Smolka and Hemmi, 2009; Zeil and Al-Mutairi 1996; Land and Layne 1995a; Zeil et al. 1986). Furthermore, the ratio of vertical and horizontal sampling resolution in *T. flammula* matches well with previously published data (Zeil et al., 1986). Equally, our calculated sampling resolution in *N. granulata also* closely matches the results of previous direct optical measurements from this species (De Astrada et al., 2012). However, our data suggest that the visual streak is much narrower (FWHM 5° vs 22°-34°) and has a higher peak of vertical resolution than the previous measurements from this animal (1.8 c/° vs 1.26 c/° in front, and 1.6 c/° vs 1 c/° in the lateral). Although individual variations are expected among crabs, this difference is most likely due to the spatial averaging of interommatidial angles inherent in the pseudopupil method. In fact, if we filter our results with an averaging window of 10° (Figure 8A), we obtain vertical resolutions (1.1 c/° front, 1.02 c/° lateral) and width of the visual streak (FWHM 20°) similar to measurements by De Astrada et al. (2012). Such a difference in the width of visual streak is not prominent in fiddler crabs data due to the presence of the secondary streak, which widens the streak considerably. Our calculations of horizontal resolution also show similar trends and values to previous pseudopupil measurements (De Astrada et al., 2012). The only real difference between our results and the ones that are previously reported for *N. granulata* (De Astrada et al., 2012) is the location of the visual streak. While our results place the visual streak at 10° above the horizon, this location is reported to be on the horizon by De Astrada et al. (2012). The only possible damage in the preparation of tissue for microCT imaging that could cause such a uniform shift of the visual streak would be a 10° movement of the rhabdom with respect to cornea. However, as argued

above, the optical axes of the ommatidia that form the visual streak are very close to perpendicular to the local curvature (Figure 6F), making such a uniform shift of the ommatidial axes seem unlikely. Additionally, our back-projection of sampling resolution to the eye (Figure 6C) shows that the visual streak is indeed formed by the ommatidia close to the dorsal part of the eye. As described in the method section, we identify the location of visual streak only by rotation of the eye so the streak's plane becomes horizontal (no translation is involved in this process). This means there is no room in our method to influence the vertical location of the streak. However, unless all the pseudopuil measurements are taken in the same animal using the same orientation of the eye in the set-up (Smolka and Hemmi, 2009), those methods do require a manual alignment of the transects. Additionally, the position of the pseudopupil is generally recorded as its centre but, where interommatidial angles change rapidly (such as on the visual streaks), the pseudopupil becomes (possibly highly) asymmetric (Land, 1997) making it difficult to identify its centre and true position. It is not clear at this stage whether these considerations can explain the differences, and further investigations will be required, including multiple measurements from the same species, and preferably a careful physiological study of sampling resolution.

Our calculation of facet diameters and optical resolutions show similar patterns in all three animals. The ommatidial facet diameter, and therefore optical resolution of ommatidia in fiddler crabs compound eye depends linearly on the size of the eye and thus the size of the crab (Smolka and Hemmi, 2009). As anticipated, the larger *T. flammula* (31.3 mm carapace length) and *N. granulata* (28 cm) generally have larger facets than *G. dampieri* (19.5 mm). Despite this difference, in all sampled individuals the highest optical resolution appears about 5° above the horizon on the lateral side of the eye (Figure 6 and 7, Supplementary Material, Figures S3-4; note that colour bars have different scales for different animals), analogous to the optical resolutions mapped across the visual fields of *G. vomeris* (Smolka and Hemmi, 2009) and *N. granulata* (De Astrada et al., 2012). This increase in the optical resolution in the lateral visual field was hypothesized to serve to detect intruding crabs (Smolka and Hemmi, 2009) or to control visually guided escape away from a predator (De Astrada et al., 2012).

4.2. The second visual streak

The major difference between our results and previously published data of fiddler crabs is the presence of two parallel, horizontal streaks in both *G. dampieri* (Figure 4) and *T. flammula* (Figure 5A, B). Previous studies which used the pseudopupil method have revealed only one prominent visual streak in five species of fiddler crabs (*G. vomeris*, Smolka and Hemmi, 2009; *Austruca lactea* Zeil and Al-Mutairi 1996; *Leptuca pugilator*, Land and Layne 1995a; *T. flammula*, Zeil et al. 1986).

We would argue that this is mainly due to the fact that the pseudopupil method is simply not sensitive enough to detect subtle differences in ocular morphology. The main reason the pseudopupil method would have missed the presence of two closely positioned streaks is that it effectively averages across 10-20 degrees of visual space. The pseudopupil is generally composed of 10's or 100's of ommatidia (Figure 8D, also see De Astrada et al., 2012; Smolka and Hemmi, 2009; Zeil et al. 1986), depending on the numerical aperture (or angular aperture) of the viewing microscope and the average interommatidial angle. Indeed, if we apply an averaging filter with the window of 10° (equal to a numerical aperture of 0.09) to the vertical sampling resolution of *G. dampieri* and *T. flammula* the secondary streak disappears in both animals (Figure 8 B, C). Detecting the secondary visual streak with pseudopupil method would be possible only with a very small microscope numerical aperture (less than 0.035) so that only one or a few ommatidia contribute to the image of the pseudopupil (instead of the 10's-100's that are commonly imaged).

In addition to this limitation of the pseudopupil method, previously published data on fiddler crabs utilized subsampling of the ommatidia to map the visual field of the animal. Zeil et al. (1986) examined the pseudopupil at 13.9 ° intervals (elevation angles) and both Smolka and Hemmi (2009) and Zeil and Al-Mutairi (1996) measured at 5° intervals (elevation angles). Given that the two visual streaks are separated by approximately 10° in elevation neither of these sampling regimes would be sufficient to reveal the two visual streaks. Furthermore, mapping ~10,000 ommatidia to estimate the full visual field in a live animal is practically impossible as the optics of the eye start to degrade within hours, which reduces the accuracy of *in vivo* measurements.

4.3. The implications of a second visual streak

Significant events in the life of crabs occur within a narrow horizontal strip of the visual world, approximately 10° above and below the horizon (Zeil and Al-Mutairi 1996). The two visual streaks that we found in both *G. dampieri* and *T. flammula* are both located in this region. Birds, which comprise the majority of fiddler crabs' predators, are larger than the fiddler crabs themselves, and often fly a few meters above the mudflat (Land 1999). The presence of a high acuity visual streak above the horizon (Figure 4-5) probably serves to detect movement, or changes in height of such possible threats. On the other hand, because fiddler crabs carry their eyes on stalks, these crabs see the bodies of other crabs below the horizon (Layne et al., 1997). Therefore, we hypothesize that the function of the second visual streak (the more ventral one) is to identify and interpret the movements of conspecifics.

While we observed two distinct visual streaks in both *G. dampieri* and *T. flammula*, there are two main differences between them. The primary visual streak (the streak with higher resolution) is the dorsal streak in *G. dampieri*, but is the ventral streak in *T. flammula*. In addition, the more ventral (secondary) visual streak in *G. dampieri* is located below the visual horizon (-8°) while in *T. flammula* the more ventral (primary) streak sits on the visual horizon. Although the difference between the species might be one reason for this variation, another explanation could reflect a difference between the sexes. Males are usually bigger than females, so they appear, on average, higher in the visual field of the female. Moreover, the males of some fiddler crab species (e.g. *Austruca lactea* and *Leptuca beebei*) build hoods of sand to advertise their burrows (Christy, 1988). Males also usually attract females by waving movements of their enlarged claw which can appear on the visual horizon (or slightly above) from the point of view of a female crab (Christy 1995; Land and Layne 1995a). Therefore, female fiddler crabs may benefit from visual streaks higher in elevation than are found in males and the relative strength of the two streaks may also reflect different pressures between the sexes. However, further research will be required to test whether these differences reflect individual variations, species, or sex specific differences.

4.4.Eyestalk, eye shape and the location and number of visual streaks

In contrast to the fiddler crabs, we only found one streak in *N. granulata*. The main difference between these animals is the position and length of their eye stalks (De Astrada et al., 2012; Zeil et al., 1986). *N. granulata* have much shorter eye stalks and keep their eyes much further

apart. This is associated with increased complexity of habitat and a higher ratio of horizontal to vertical resolution (Zeil et al., 1986). This suggests *N. granulata* has a much higher selection pressure on horizontal resolution, which will limit their capacity to elongate the eye, reducing their capacity to develop a second visual streak. In addition, the eyes are so close to the body, that *N. granulata* would often see the bodies of other crabs above the horizon. Therefore, moving the visual streak to a higher position in the visual field may allow them to more easily separate conspecifics from predators (Layne et al., 1997). A similar energy or eye space constraint may limit *G. dampieri* to develop a higher visual streak like the other two species. It would require *G. dampieri* to further elongate its eye.

Equally, another argument for presence of two visual streak in the *T. flammula* eye would be the elongation of the eye. *T. flammula* (Figure 6B) has the most elongated eye of all three species we examined. Given the location of the ommatidia that form the primary streak on the eye in this animal (Figure 6B), more than half of the eye space is invested above this primary visual streak. It would be surprising if the animal invested so much eye space and energy (Niven and Laughlin, 2008) without any increase in visual resolution in a zone of the eye that is relatively small and low resolution in all other species that have been examined so far.

However, the interactions between eye shape, behaviour and the cost of visual systems are very complicated. It is not clear at this stage whether these can explain the differences between different animals, or they are artefacts of fixation. Further investigations will be required to identify the cause of these differences.

4.5.Effectiveness of the method

Despite the advantages of this method it is sensitive to sample preparation. Using Agarose or similar protective gels to hold the eye still during the scanning process can eliminate some sources of damage, but care is essential in handling the samples. Although this method is still time consuming, recent advances in the field of computer image analysis may make it possible to process microCT images in an automated or semi-automated manner using computational neural network techniques to find the centres of the corneas and rhabdoms. This is the current focus of our work.

In conclusion, the results obtained from our new method agree well with previous measurements in both *N. granulata* and a closely related fiddler crab. Additionally, it provides further details about the visual field by eliminating the subsampling of ommatidia which is almost unavoidable with previous methods. However, since we only measured one animal of

each species, we cannot conclusively confirm these new details and repeat measurements from the same sex and species are required. This would be achievable by automation of the method and, once automated, it will be possible to rapidly employ the method to any apposition compound eye, regardless of its shape or complexity. Because it can be used on appropriately preserved samples, there also exists the prospect of applying it to animals that are impossible to maintain alive for study including those that live in unique and inaccessible environments such as deep-sea crustaceans. Moreover, this method does not require any specialized optics, or complex preparation of samples, and microCT systems are now commonplace in most research institutions.

Acknowledgement

This research was supported under Australian Research Council's Discovery Projects funding scheme (project number DP170104131). We are grateful to Dr Martín Berón de Astrada and Professor Daniel Tomsic for their assistance with supplying and preparing *Neohelice granulata* sample and Dr Martín Berón de Astrada for insightful discussions. We thank Zohria-Lys Guillerm for her help with manually labelling the ommatidia. The authors acknowledge the facilities, and the scientific and technical assistance of Microscopy Australia at the Centre for Microscopy, Characterisation & Analysis, The University of Western Australia, a facility funded by the University, State and Commonwealth Governments.

Author Contributions

Z.M.B. helped with labelling microCT images and developed the analysis software. She analysed and interpreted the data and drafted the manuscript. A.L.J, Y.O and J.S prepared and scanned the samples and helped draft the manuscript. S.K. labelled microCT images and helped draft the manuscript. J.C.P was involved in scanning the eyes and co-authored the manuscript. J.M.H developed the manual labelling software. He helped with labelling microCT images, analysing, interpreting the data, and drafting the manuscript.

Declaration of Interests

The authors declare no competing interests.

References

Bergman M and Rutowski RL (2016) Eye morphology and visual acuity in the pipevine swallowtail (*Battus philenor*) studied with a new method of measuring interommatidial angles. Biological Journal of the Linnean Society, vol. 117, no. 3, pp. 646-654.

Christy JH (1988) Pillar function in the fiddler crab *Uca beebei*. II. Competitive courtship signalling. Ethology 78, 113–128.

Christy JH (1995) Mimicry, mate choice and the sensory trap hypothesis. The American Naturalist, 146(2), pp.171-181.

Dahmen H (1991) Eye specialisations in water striders: an adaptation to life in a flat world. Journal of Comparative Physiology A, 169(5), pp.623-632.

De Astrada MB, Bengochea M, Medan V and Tomsic D (2012) Regionalization in the eye of the grapsid crab Neohelice granulata (= Chasmagnathus granulatus): variation of resolution and facet diameters. Journal of Comparative Physiology A, 198(3), pp.173-180.

Garcia D (2010) Robust smoothing of gridded data in one and higher dimensions with missing values. Computational Statistics and Data Analysis, 54(4), pp.1167-1178.

Horridge GA (1978) The separation of visual axes in apposition compound eyes. Philosophical Transactions of the Royal Society of London B, 285(1003), pp.1-59.

Kirschfeld K (1976) The resolution of lens and compound eyes. In Neural Principles in Vision (pp. 354-370). Springer, Berlin, Heidelberg.

Land MF (1981) Optics and vision in invertebrates. Handbook of Sensory Physiology Vol VII/6B, pp.471-592.

Land MF (1989) Variations in the structure and design of compound eyes. In Facets of vision, Springer Berlin Heidelberg, 90-111.

Land MF (1997) Visual acuity in insects. Annual review of entomology, 42(1), pp.147-177.

Land MF (1999) The roles of head movements in the search and capture strategy of a tern (Aves, Laridae). Journal of Comparative Physiology A, 184:265–272.

Land M, Layne J (1995) The visual control of behavior in fiddler crabs. I. Resolution, threshold and the role of the horizon. Journal of Comparative Physiology A, 177:81–90.

Land M, and Nilsson DE (2012). Animal eyes. Oxford: Oxford University Press.

Layne J, Land M and Zeil J (1997) Fiddler crabs use the visual horizon to distinguish predators from conspecifics: a review of the evidence. Journal of the Marine Biological Association of the United Kingdom, 77(1), pp.43-54.

Nalbach HO, Zeil J and Forzin L (1989) Multisensory control of eye-stalk orientation in space: Crabs from different habitats rely on different senses. Journal of Comparative Physiology A, 165, 643-649.

Niven J.E. and Laughlin S.B (2008) Energy limitation as a selective pressure on the evolution of sensory systems. Journal of Experimental Biology, 211(11), pp.1792-1804.

Schwind R (1980) Geometrical optics of the Notonecta eye: adaptations to optical environment and way of life. Journal of Comparative Physiology, 140(1), pp.59-68.

Smolka J and Hemmi JM (2009) Topography of vision and behaviour. Journal of Experimental Biology, 212(21), pp.3522-3532.

Snyder AW (1979) Physics of vision in compound eyes. In Comparative Physiology and Evolution of Vision in Invertebrates (pp. 225-313). Springer, Berlin, Heidelberg.

Stavenga, D. G. (1979). Pseudopupils of compound eyes. In Handbook Of Sensory Physiology, vol. VII/6a (ed. H. Autrum), pp. 357-439. Berlin, Heidelberg, New York: Springer.

Stavenga DG (2003a). Angular and spectral sensitivity of fly photoreceptors. I. Integrated facet lens and rhabdomere optics. Journal of Comparative Physiology A, 189, 1-17.

Stavenga DG (2003b). Angular and spectral sensitivity of fly photoreceptors. II. Dependence on facet lens F-number and rhabdomere type in *Drosophila*. Journal of Comparative Physiology A 189, 189-202.

Stavenga DG (2004) Angular and spectral sensitivity of fly photoreceptors. III. Dependence on the pupil mechanism in the blowfly Calliphora. Journal of Comparative Physiology A, 190, 115-129.

Straw AD, Warrant EJ and O'Carroll DC (2006) A bright zone in male hoverfly (Eristalis tenax) eyes and associated faster motion detection and increased contrast sensitivity. Journal of Experimental Biology, 209(21), pp.4339-4354.

Taylor GJ, Tichit P, Schmidt MD, Bodey AJ, Rau C and Baird E (2019) Bumblebee visual allometry results in locally improved resolution and globally improved sensitivity. eLife, 8, p.e40613.

Van Hateren JH, Hardie RC, Rudolph A, Laughlin SB and Stavenga DG, 1989. The bright zone, a specialized dorsal eye region in the male blow fly Chrysomyia megacephala. Journal of Comparative Physiology A, 164(3), pp.297-308.

Warrant EJ and McIntyre PD (1993) Arthropod eye design and the physical limits to spatial resolving power. Progress in Neurobiology, 40(4), pp.413-461.

Zeil J, Al-Mutairi MA (1996) The variation of resolution and of ommatidial dimensions in the compound eye of the fiddler crab Uca lactea annulipes (Ocypodidea, Brachyura, Decapoda). Journal of Experimental Biology, 199(7), pp.1569-1577.

Zeil J and Hemmi JM (2006) The visual ecology of fiddler crabs. Journal of Comparative Physiology A, 192(1), pp.1-25.

Zeil J, Nalbach G, Nalbach HO (1986) Eyes, eyes stalks and the visual world of semi-terrestrial crabs. Journal of Comparative Physiology A, 159(6), pp.801-811.

Figures

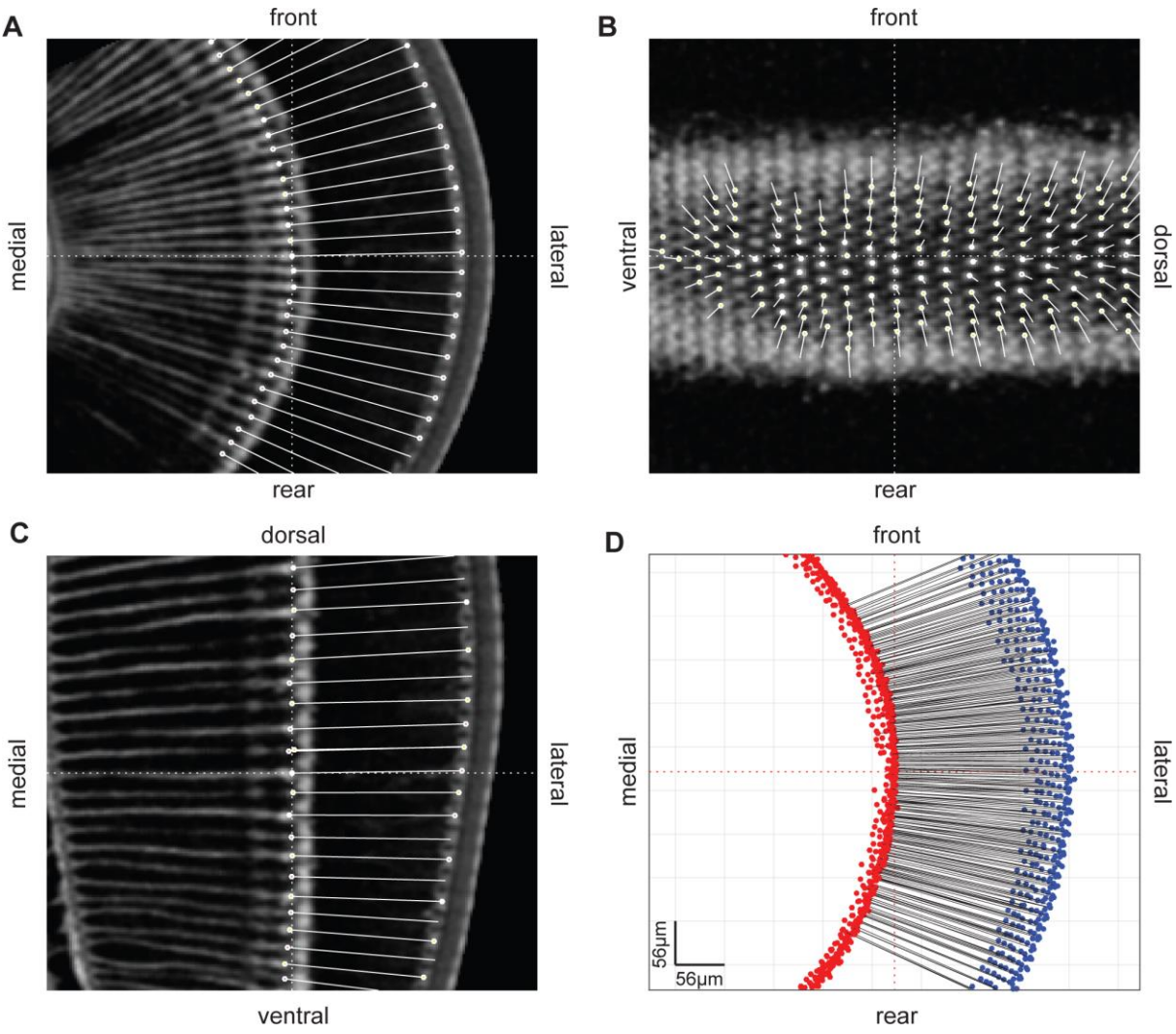

Figure 1. 2- and 3-dimensional reconstructions of the ommatidial axes of *G. dampieri* (A, B, C) The centres of each cornea and the tip of the corresponding rhabdoms (shown by points) were labelled by viewing microCT images of compound eyes in three perpendicular planes. The two corresponding points identify the optical axis of the crystalline cones (solid lines) (A) Horizontal plane (perpendicular to the eye stalk, approximately through the middle of the eye), (B&C) Vertical planes through the mid-point in (A) as marked by the dotted crosshairs. Section B shows the tip of rhabdoms and the base of the crystalline cones and shows how the axes of these lenses diverge along the horizontal direction. (D) The coordinates of the centres of the corneas (blue points), rhabdoms (red points) of the ommatidia visible in A (and their neighbours), and the optical axes of ommatidia, as calculated based on these points in 3-dimensional space.

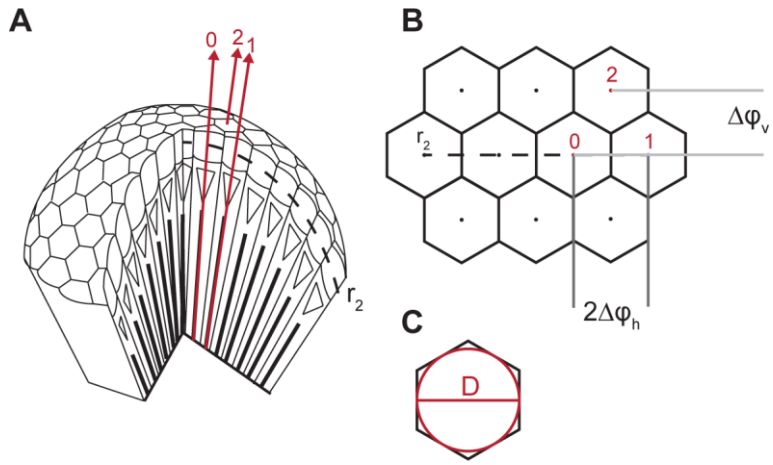

Figure 2. Calculation of interommatidial angles and facet diameter. (A) Schematic of compound eye showing the arrangement of a horizontal row (r_2) and optical axes of three ommatidia (red arrows labeled as 0, 1, 2). The optical axis of each ommatidium was determined by calculating the vector connecting the center of cornea and distal tip of the rhabdom. (B) a magnified top view of (A) showing the vertical angular distance between the optical axis of ommatidia in consecutive horizontal rows ($\Delta\varphi_v$, vertical interommatidial angle) and the horizontal angular distance between optical axis of ommatidia in these rows ($2\Delta\varphi_h$, twice the horizontal interommatidial angle). (C) The facet diameter, was estimated as the diameter of the incircle of hexagon which was calculated as the average distance of the centre of the focal facet from the centres of its six neighbours.

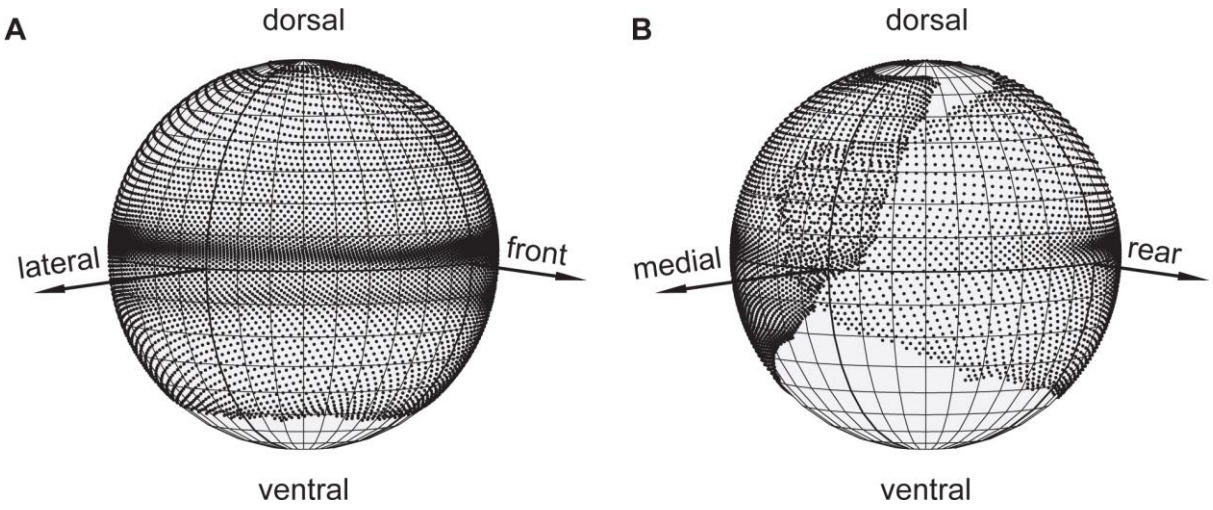

Figure 3. The visual field of the right eye of *G. dampieri*. Black dots represent the directions of the mapped optical axes of ommatidia into the surrounding sphere, as if they emanate from the centre of the sphere. Horizontally, the visual field covers a full 360º field of view with ~30º overlap in the medial area. (A) The visual streak is most prominent in the frontal part of the eye but is evident throughout the fronto-lateral eye. Another, secondary streak is visible just below the visual horizon (B) In the medial part of the visual field, the viewing directions of ommatidia from opposing edges of the eye overlap. The horizontal visual streak is less developed in the caudo-medial visual field.

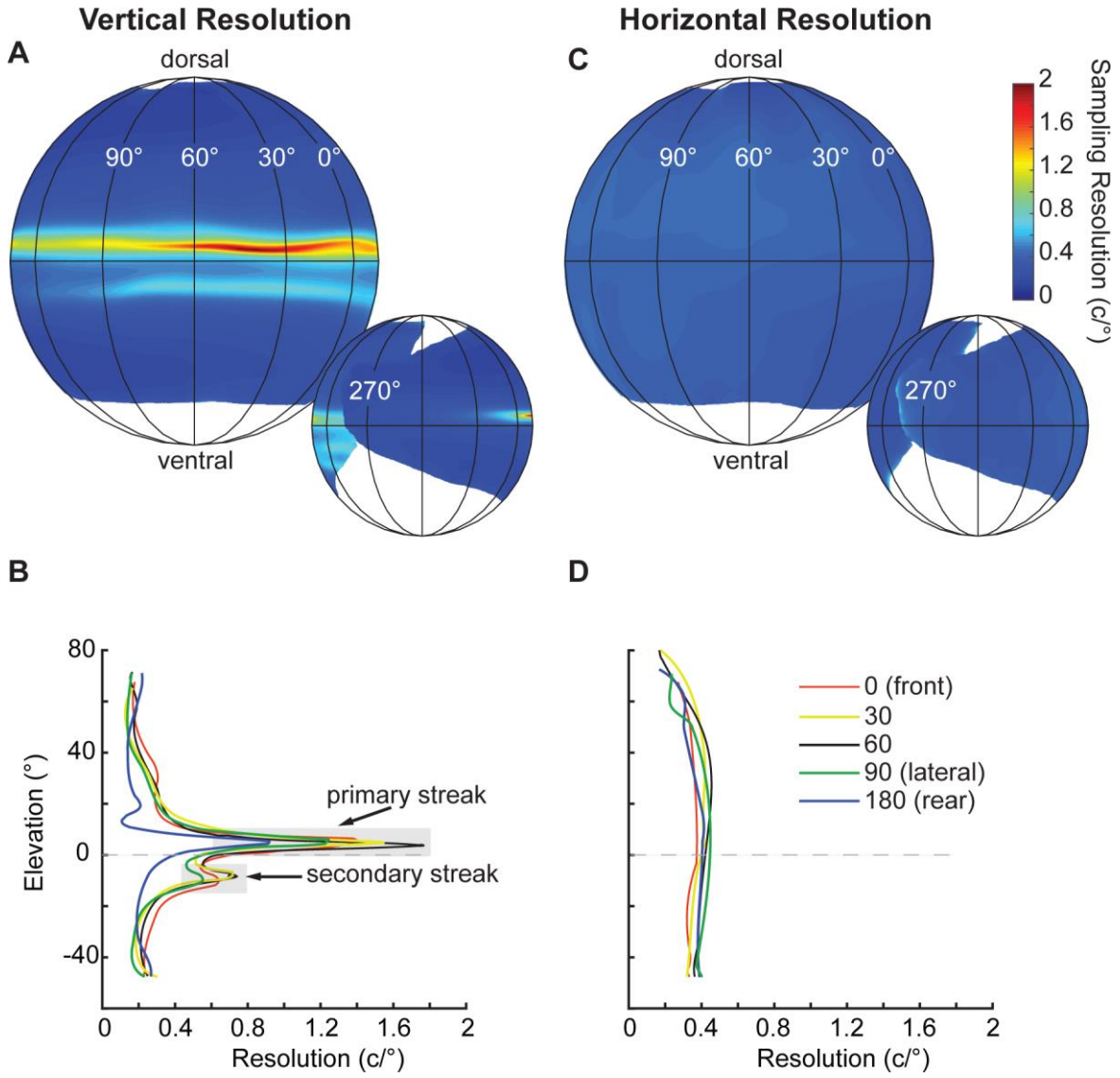

Figure 4. Variation of vertical and horizontal sampling resolution in a male *G. dampieri*. (A, B) Vertical and (C, D) horizontal sampling resolution on spherical maps (A, C) and vertical transects (B, D). The horizontal resolution remains fairly even across the eye. The two distinct visual streaks of vertical resolution are located on 5° (primary streak) and -8° (secondary streak) of elevation.

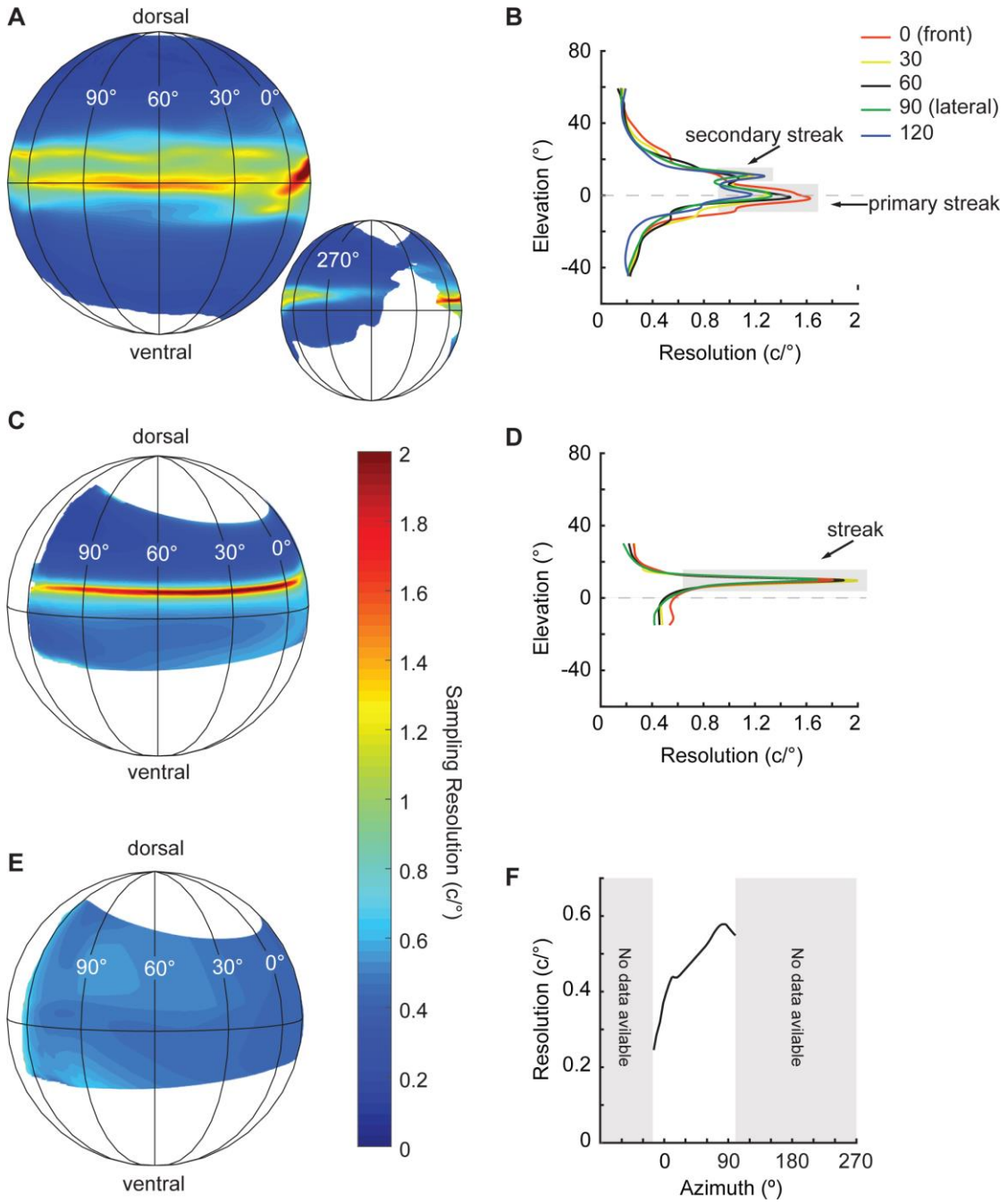

Figure 5. **Sampling resolution in *T. flammula* and *N. granulata*.** (A) The spherical map and (B) vertical transects of vertical sampling resolution clearly show two visual streaks in *T. flammula*. In contrast to *G. dampieri*, the primary streak is found at the lower elevation (0°) compared to the secondary streak, which is found more dorsally (at 10° of elevation). (C) Vertical sampling resolution and (D) vertical transects in *N. granulata* show the presence of only one visual streak at 10° above the horizon. (E) The horizontal resolution of *N. granulata* is not uniform and increases towards lateral part of the eye. (F) A horizontal transect of horizontal resolution at 10° of elevation.

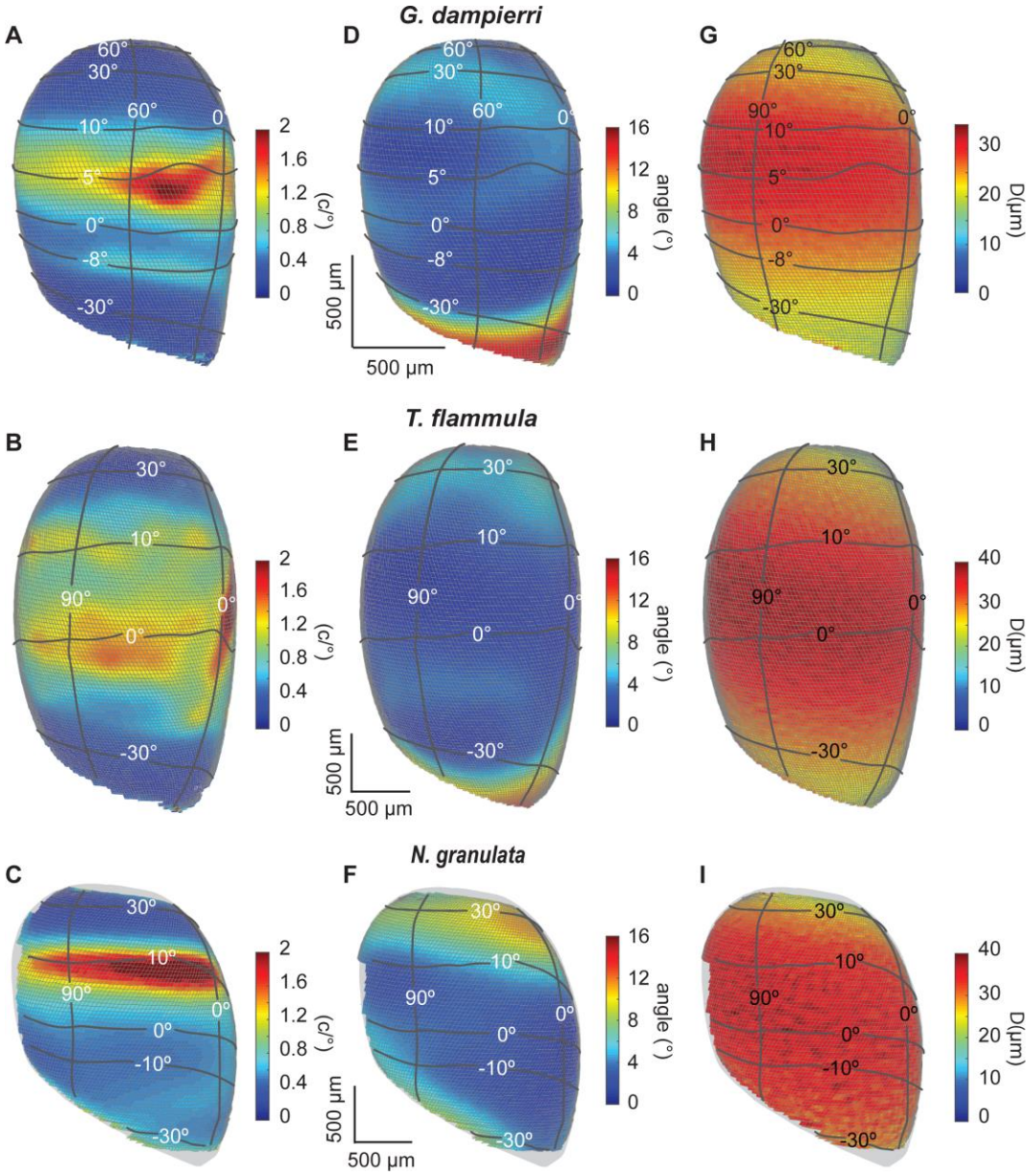

Figure 6. Resolution, the direction of ommatidia in relation to local eye curvature, and facet size. (A, B, C) Back projections of vertical sampling resolution on the eyes of (A) *G. dampieri*, (B) *T. flammula*, (C) *N. granulata* shows the location of the ommatidia that form the visual streak on the eye. (D, E, F) The angular differences between the ommatidial axes and the local surface normal indicate that in all three animals the visual streaks is located in the flat part of the eye where the ommatidial axis are closely aligned with the local surface normal (<3deg). (G, H, I) The biggest facets are located at approximately 5° above the horizon in the lateral part of the eye, approximately in the middle of the elongated eye space. The grey surface underneath the map of *N. granulata* shows the complete outline of the eye.

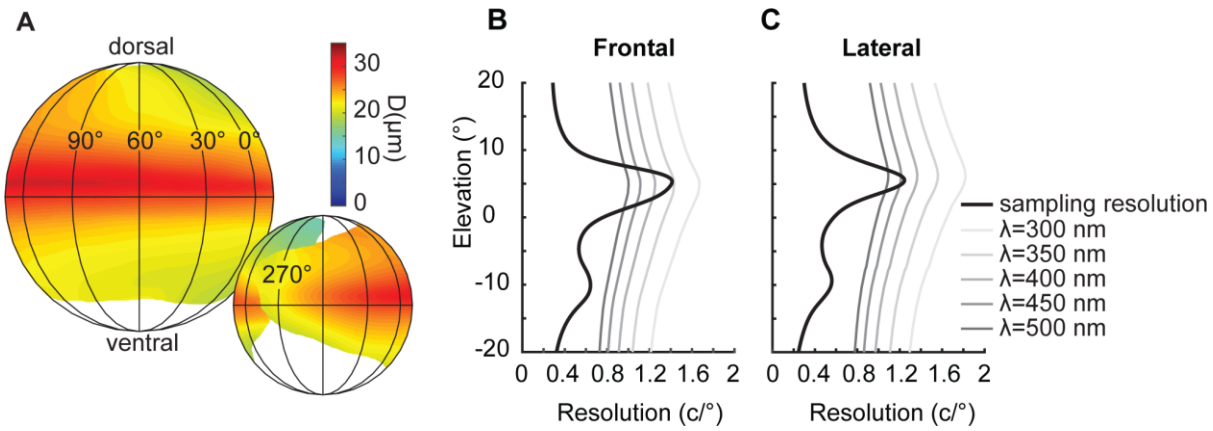

Figure 7. Facet diameter and optical resolution in the male *G. dampieri*. The variation of facet diameter (A) projected onto a surrounding sphere. The facets looking in directions -5° to 20° in elevation are larger. (B, C) Comparison of vertical sampling resolution (black lines) estimated from interommatidial angles, and optical resolution (grey lines) estimated from the diameter of the Airy disk images produced by ommatidial facets and lenses, in: (B) frontal, and (C) lateral vertical transects of the eye. Optical resolution depends on the wavelength of sampled light and is shown for five different wavelengths. Direct comparison of sampling versus optical resolution suggests that the lateral region is able to resolve spatial patterns of longer wavelength than the frontal visual field.

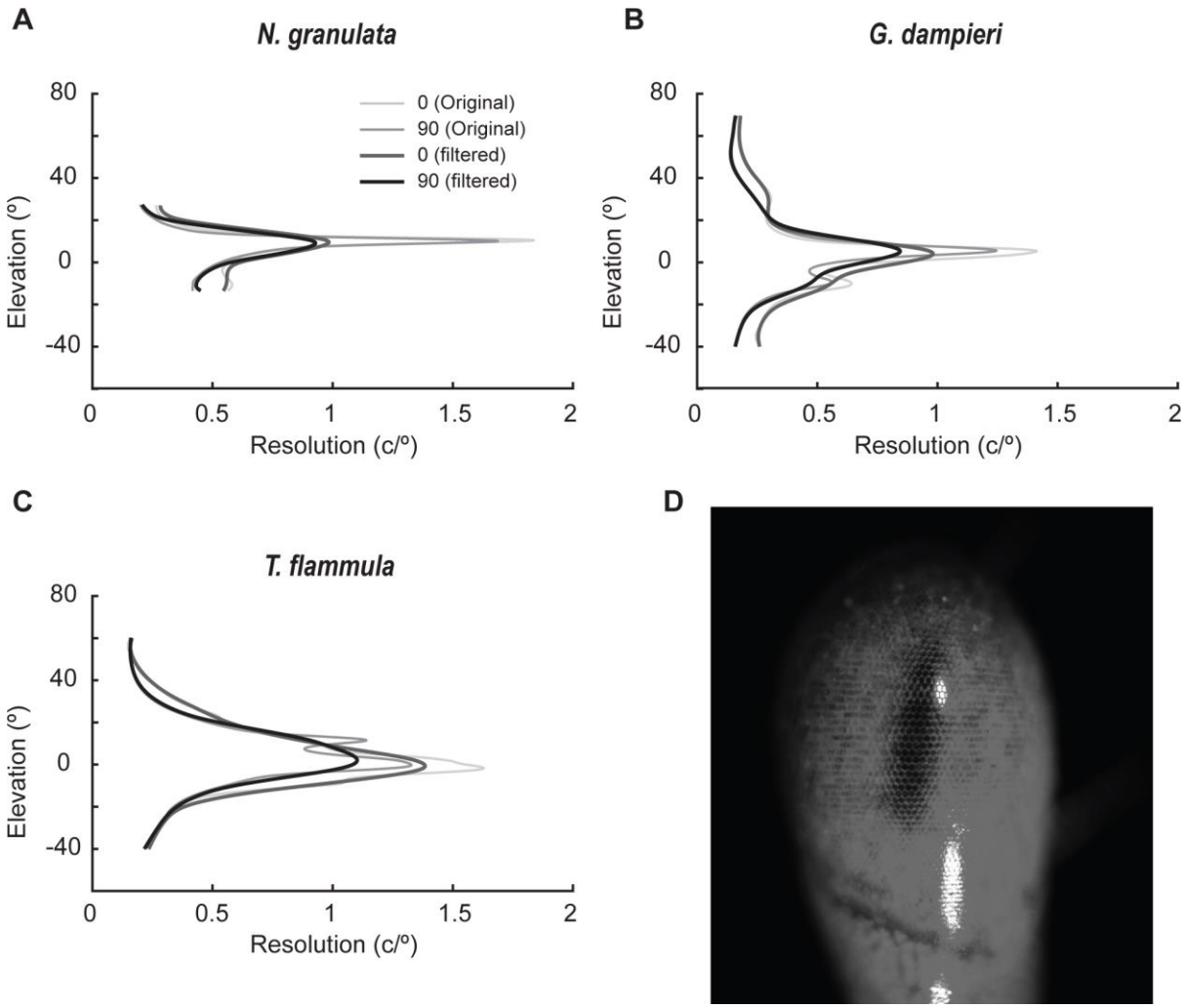

Figure 8. Spatial averaging in pseudopupil method. The vertical sampling resolution of (A) *N. granulata* (B) *G. damoieri* and (C) *T. flammula* filtered with an averaging window of 10°. This averaging which resembles the typical 10°-20° averaging of visual space by pseudopupil method diminishes the secondary visual streak in both species of fiddler crabs and results in a wider and shorter visual streak compared to the results obtained via current method. (D)The image of the pseudopupil of a *G. dampieri* is taken in the same optical set-up used by Smolka and Hemmi (2009) which employed a microscope with a numerical aperture of 0.1. The pseudopupil image is composed of approximately 85 ommatidia and has an indistinct boundary. The centre of the pseudopupil needs to be defined, and located, in order to map its position across the eye.

Supplementary Material

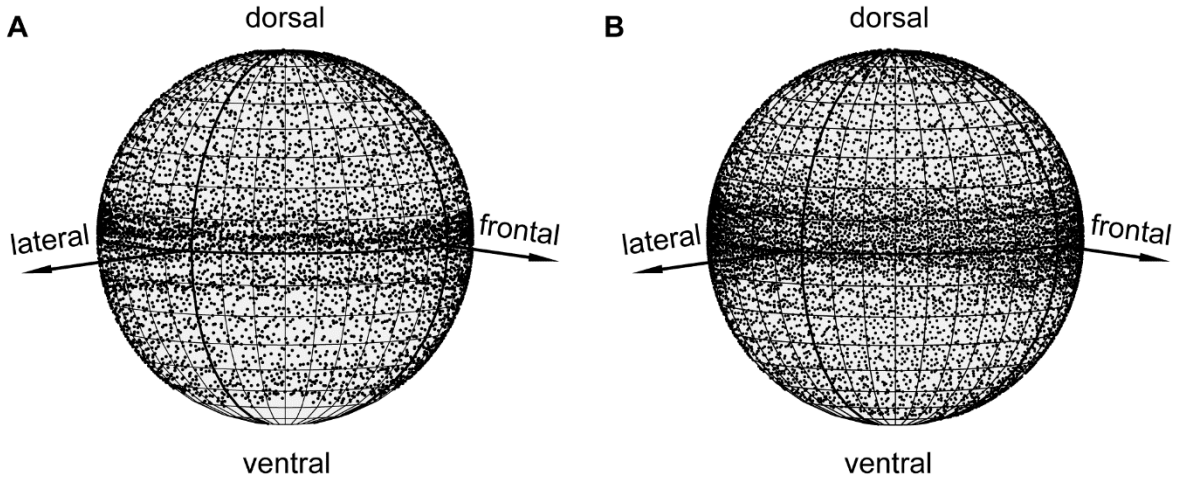

Figure S1. The raw (unsmoothed) visual field. The visual field of (A) the right eye of a male *G. dampieri* and (B) the right eye of a female *T. flammula*. Black dots represent the optical axis of each ommatidium mapped onto a surrounding sphere, the eye being assumed to be at the centre of the sphere and infinitely small. Two visual streaks are observable in both animals in the unsmoothed data as well as in smoothed representations (Figure 3 and Figure S3).

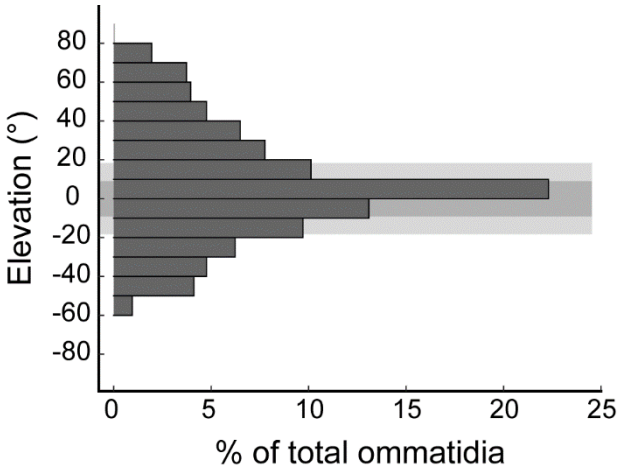

Figure S2. Distribution of elevation viewing directions in *G. dampieri*. 30% of the total of 9715 ommatidia are looking at ±9º of elevation (dark grey band) and 50% are devoted to ±18º of elevation (light grey band) illustrating the importance of the visual horizon for fiddler crabs.

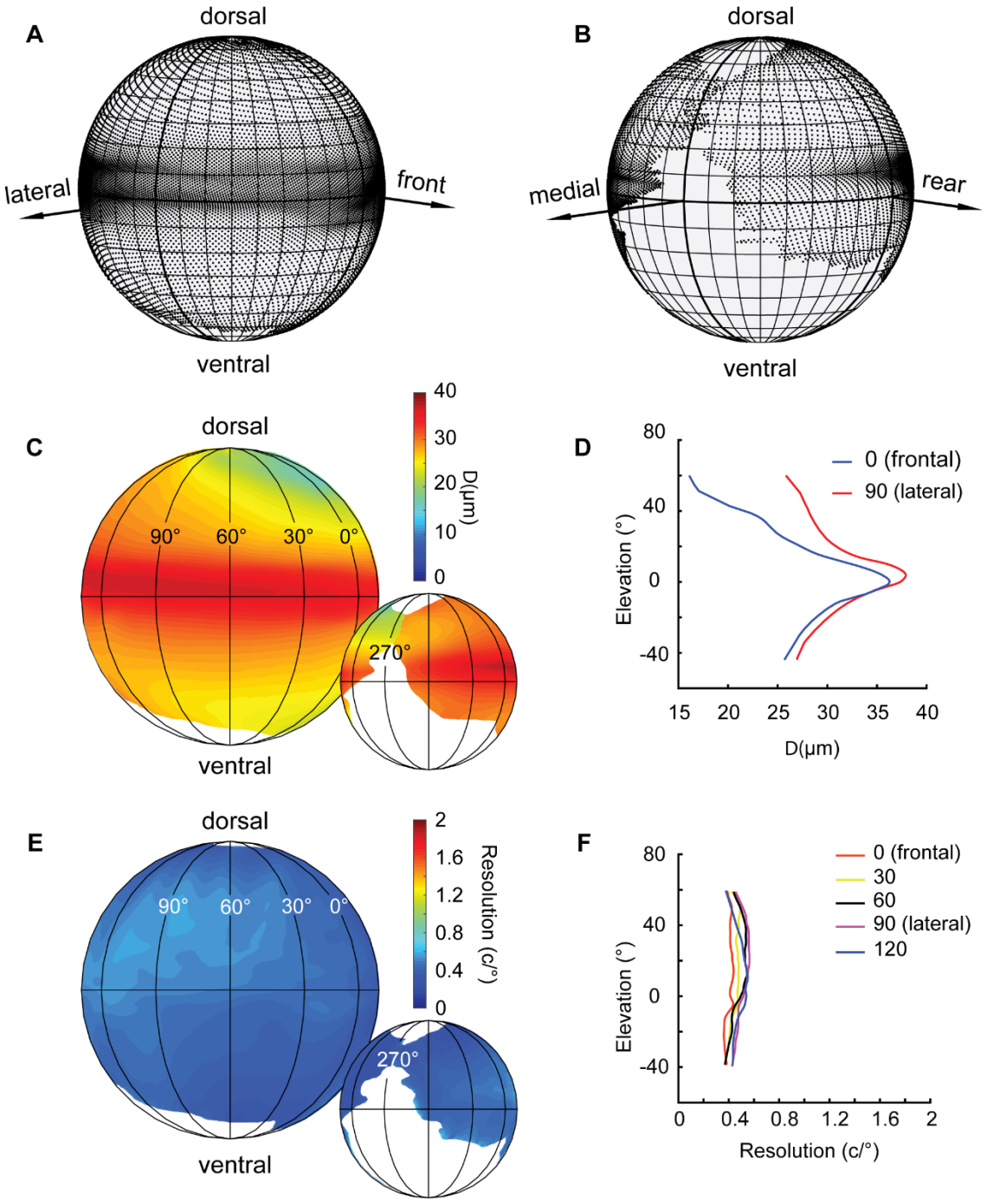

Figure S3. Analysis of the right eye of the female *T. flammula*. (A, B) The visual field showing the projections of ommatidia onto a surrounding sphere**.** Black dots represent the mapped optical axis of each ommatidium into the surrounding sphere. Two streaks of high sampling are noticeable along the horizon, extending through most of the horizontal field of view. Please note that the reconstruction of the eye is not complete in the medial area of the eye, hence the larger gap in that eye region compared to *G. dampieri.* (C) The variation of facet diameter projected onto a surrounding sphere. (D) Two vertical transects of facet diameters in the front and lateral visual fields. The largest facets project predominantly around 5° above the horizon of the visual field. The female *T. flammula* has larger facets than the male *G. dampieri* (Fig. 7. Note the different scale on colour bar used in the figures for these two animals). (E) Spatial distribution of horizontal sampling resolution as a spherical map and (F) vertical transects of horizontal sampling resolution at several positions in azimuth. Horizontal resolution remains relatively constant across the visual field.

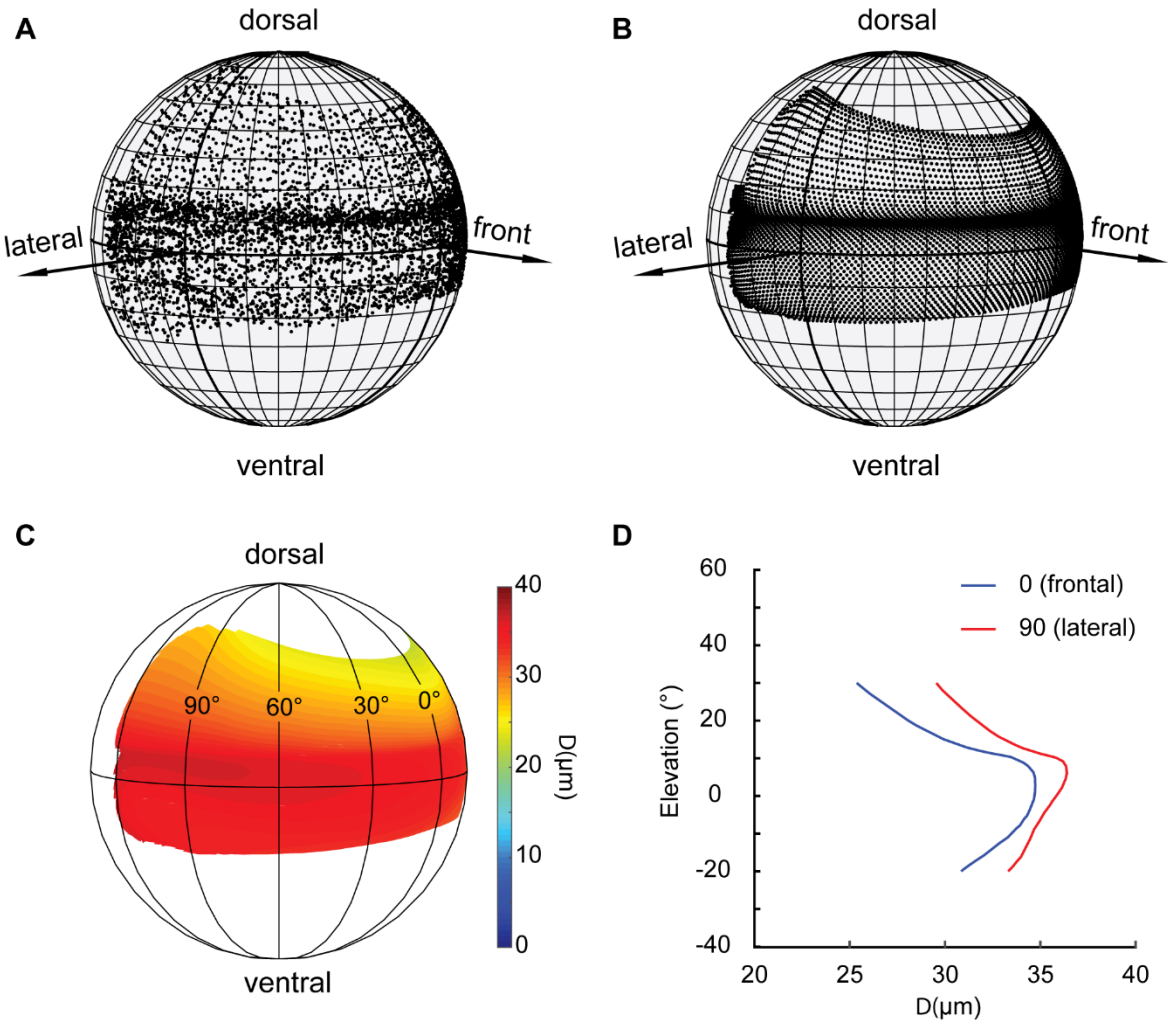

Figure S4. Analysis of the right eye of the male *N. granulata*. (A) The raw (unsmoothed) and (B) smoothed map of optical axis of (marked) ommatidia projected onto a surrounding sphere, the eye being assumed to be at the centre of the sphere. Only one visual streak is observable in both the unsmoothed and the smoothed representation. (C) The variation of facet diameter in spherical view, and (D) frontal and lateral vertical transects of facet diameter. The largest facets are found between 5° and 10° above the horizon in the lateral visual field and between 0° and 10° in the frontal visual field.